Out-of-plane ply wrinkling defects during consolidation over an external radius*

T. J. Dodwell, R. Butler, G. W. Hunt
Department of Mechanical Engineering, University of Bath, Claverton Down, Bath, UK

10th June 2014

Abstract

If carbon fibre layers are prevented from slipping over one another as they consolidate onto a non-trivial geometry, they can be particularly susceptible to wrinkling/buckling instabilities. A one dimensional model for out-of-plane ply wrinkling during consolidation over an external radius is presented. Critical conditions for the appearance of wrinkles provide manufacturing strategies to eliminate such defects. Predicted wrinkle wavelengths and critical wrinkling conditions show good agreement with wrinkle defects observed in a spar demonstrator.

Keywords: A. Layered Structures, B. Defects, C. Modelling, Wrinkling

1 Introduction

Whilst the basic advantages of composite laminates are well proven, they are often compromised by high costs, long development time, and poor quality due to multiple defects, particularly in massive complex parts such as those found in aerospace applications. The modelling, simulation and optimisation of manufacturing processes therefore has widespread applications to the industry, with the twin objectives of improving product quality and decreasing production time.

1.1 Wrinkling of carbon fibre composites during consolidation

Typically, carbon fibre composite parts are made by layering a series of thin carbon fibre layers, pre-impregnated with resin, onto a tool surface. During this lay-up process the stack of plies is consolidated at moderate temperatures and pressures to remove air trapped between layers. This debulking process aims to ensure correct seating onto the tool surface, and to promote adhesion between plies. However, as a laminate consolidates over even a simple geometry the plies are forced to accommodate the imposed geometry of the tool surface. For example, consider consolidation over an external radius Fig. 1 (left). As the outermost ply consolidates it is forced into a tighter geometry; if the layers cannot shear relative to one another, they are put into axial compression. For plies in which the fibres align with this stress, their stiffness is particularly high. If layers can shear/slip over one another the additional length can be accommodated by producing so called 'book-ends'. If the resistance is too high, layers may form wrinkles. Figure 1 (right) shows small amplitude wrinkles or folds, which have developed in the corner radius of a large scale component. Understanding how wrinkles form during these manufacturing processes is important because, depending on their severity, they may compromise the structural integrity of the final part, leading in some cases to expensive wholesale rejection. The formation of wrinkles not only disrupts the even distribution of fibre and resin, but most significantly can increase through-thickness stresses triggering failure at significantly reduced loads [1].

A distinction is made between *ply* and *fibre wrinkling*. In this contribution the former are observed in Fig. 1 (right), in which the ply deforms as an integral layer rather than independent fibres. The bending stiffness of a ply is much greater than that of a single fibre; consequently wrinkles in plies form over much longer wavelengths than those observed in fibres. Ply wrinkling occurs predominately in pre-impregnated materials in which each ply is laid down as an integral layer, as opposed to infusion based manufacturing processes. The thickness of a typical pre-impregnated ply is much smaller than the width, and therefore the bending stiffness out-of-plane is much smaller than in-plane. Consequently ply wrinkling is predominately out-of-plane; unlike fibre wrinkling where rotational symmetry of a single fibre means there is no preferential wrinkling direction. Various experimental contributions have considered fibre wrinkling [18, 8] and to a lesser extent ply wrinkling; for example Lightfoot *et al.* [15] considered ply wrinkling due to shear interactions between ply and tool, whereas Hallander *et al.* [10] studied the formation of wrinkles during forming of unidirectional prepregs over complex geometries. Various

*Accepted for publication in Composite Science and Technology, October 2014.

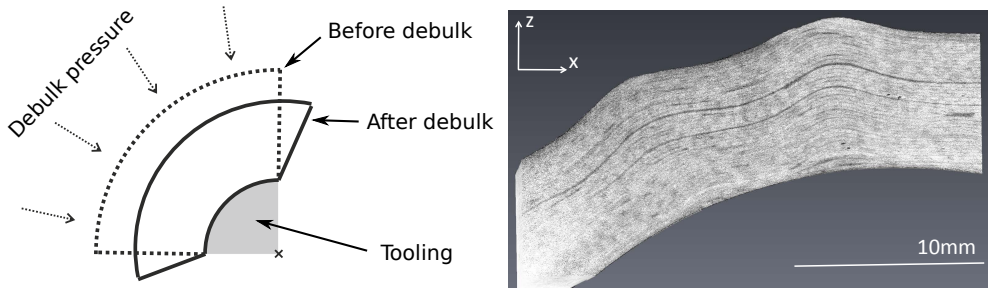

Figure 1: (Left) A representation of the *bookend* effect, created when a laminate is consolidate over a corner radius. (Right) CT image of a corner wrinkle in the $x-z$ plane of a spar demonstrator with half-wavelength of 5.47mm.

publications have focused on mechanism for fibre wrinkling, such as wrinkling due compressive loading [19] and automated fibre placement (AFP) [2]. Previous modelling of ply wrinkles has considered wrinkling of a single textile composite whilst draping over a complex geometry using traditional finite element methods [3, 22] and single ply buckling models [17]. The authors are unaware of analytical models which capture multilayered wrinkling during consolidation as studied in this contribution.

1.2 Complexities of modelling multilayered systems

The limited modelling-based work on ply wrinkling is primarily due the inherent complexities of modelling multilayered structures. In particularly the strongly nonlinear geometric constraints of layers fitting together leads to a complex mix of both material and structural type behaviour. The primary aim of this contribution is to develop an analytical approach which captures the multilayered ply wrinkling during consolidation over a non-trival geometry. Such analysis provides insight into the mechanisms and key parameters which control ply wrinkling during consolidation, leading to greater understanding than can be obtained from simple geometric observations alone.

A variety of models have been proposed for the consolidation of composite laminates. Typically, these take the form of flow-compaction continuum models, which couple a nonlinear elastic response of the fibres with a Darcy-type flow model for the redistribution of resin throughout the laminate [9, 11]. However, with finely-layered structures and uncured laminates, slip at the interfaces between layers can introduce highly nonlinear, anisotropic behaviour. Rapidly-varying shear stresses through the layer thickness, for example, can result from plies slipping and bending as individual layers rather than a combined laminate [17]. Current process models do not account for the anisotropy introduced by the layering, and as a result such models cannot capture layer-level phenomena such as wrinkling.

To include the mechanics of individual layers, explicit finite element calculations can be performed using special interface elements [21]. Any number of interfaces could be modelled this way, yet such approaches are naturally restricted since mesh sizes must be sufficiently small compared with layer thickness. Some modelling based approaches have sought to include interlayer mechanics by deriving homogenised anisotropic continuum models. Such models are effective if shear properties of the interface and the layer are similar, as for example in a cured laminate. However, for larger disparities, where the layers have the potential to undergo slip and separation, such models break down. For these cases, models must not only consider the anisotropic nature of shear at the interfaces, but also the individual contributions of layers as they bend. An *alternative approach*, taken here, is to incorporate the individual contributions of layers in bending into a variational formulation. Here the interlayer geometry can be described by front propagation techniques such as the *level set method* [4], or by assuming simplified interlayer relationships [12] as developed in this contribution.

1.3 Overview of the paper

The paper is organised as follows. In section 2 a one-dimensional model for wrinkling during consolidation over a corner radius is presented deriving a critical buckling load and wavelength for the wrinkle solutions. This analysis is extend by introducing the concept of a critical limb length, the limb length above which the part will form a wrinkle. Section 3 approximates modelling parameters for both consolidation behaviour and bending of unidirectional prepreg. The main results are presented in section 4. Firstly the buckling wavelength and the critical limb lengths are compared with wrinkles in a demonstrator spar. This is followed by a parametric study of each modelling parameter, which is then related back to manufacturing processes and design decisions. The paper concludes with some general observations, a discussion of the limitations of the model and future avenues to address open questions.

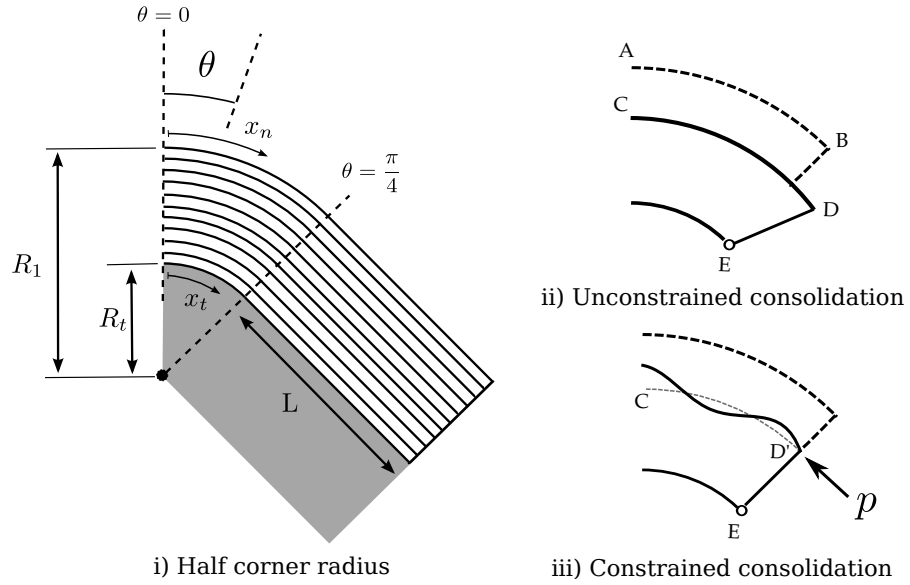

Figure 2: (i) Setup of half the corner radius, identifying a number of key geometric parameters. (ii) and (iii) show two possible scenarios as a laminate consolidates over a corner radius. If, as in (ii), layers are free to slip over one another, *book-ends* form (CDE). If this slip is prevented, as in (iii), the inextensible laminate must wrinkle ($CD'E$).

2 The wrinkling model

The model comprises a stack of N plies of uniform initial thickness h and unit width, that have been laid over a tool surface characterised by the circular arc $x_t = R_t\theta$, for θ in the range $[-\pi/4, \pi/4]$, and straight limbs of length L, see Figure 2(i). The i^{th} layer, numbering from the outside inwards, is described by a radius of curvature R_i with arc-length parameter x_i and total length $\ell_i = \frac{1}{2}\pi R_i$.

2.1 Modelling assumptions

A number of modelling assumptions are made:

- All plies are assumed to be identical and inextensible in the fibre direction;
- Only the elastic contributions of the fibres and resin are considered in the buckling formulation;
- The analysis is limited to the consolidation over a symmetric external corner radius;
- Temperature is assumed uniform and constant throughout the laminate;
- The laminate stacking sequences is taken into account by assuming a rule of mixtures;
- The laminate wrinkles as a complete laminate, with greatest amplitude on the outside and smallest on the tool surface (as seen in Fig. 1 (right)). The model does not consider modes of deformation where an individual layer or a collection of layers wrinkle independently of the whole laminate;
- The model assumes the pre-buckled state is one of uniform consolidation the corner radius, and only considers the initial bifurcation/onset of a wrinkling instability.

The true response is a complex mix of nonlinear geometry and viscoelastic, temperature-dependent rheology which is not amenable to an analytical approach, as presented here. Our objective is to develop a simplified model in which the parameters influencing the ply wrinkling can be identified and carefully monitored.

2.2 The buckling problem

A uniform debulk pressure q is first applied to the outside layer, causing the laminate to consolidate by a strain η. This then imposes the loading for the wrinkling or buckling problem. The initial consolidation of the laminate is assumed to exhibit a general nonlinear stiffening behaviour [9] given by the power law

$$q(\eta) = C\eta^2, \tag{1}$$

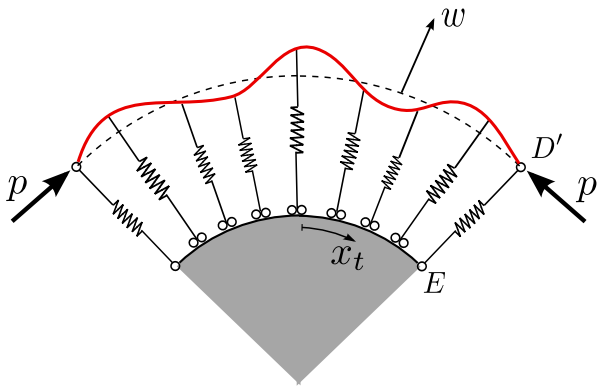

Figure 3: Setup of the buckling model, simplified to a single layer of effective stiffness $\hat{B}$, laid around the corner radius $R(\eta)$, and on a nonlinear Winkler foundation. A rigid load p prevents the laminate from producing *book-ends* and causes the laminate to wrinkle.

for a constant $C > 0$. The radius of curvature of the i^{th} layer therefore reduces during consolidation to

$$R_i(\eta) = R_t + \frac{1}{2}h(1-\eta)^2(2(N-i)+1). \tag{2}$$

The change of variable, $\mathrm{d}x_i = (R_i/R_t)\,\mathrm{d}x_t$, proves useful throughout the analysis since the tool surface x_t remains unchanged during consolidation. Consider the two scenarios depicted in Fig. 2 (ii) and (iii). If the layers are allowed to freely slip over each other, the original length AB must remain equal to the length CD, and as a result book-ends will form, as in Fig. 2 (ii). Next consider the alternative case of Fig. 2 (iii) where layers are constrained from slipping over one another. Rigid load p_i acting on layer i prevents it from slipping a distance

$$\lambda_i(\eta) = \frac{1}{4}h\pi\eta(1-\eta)\left(2(N-i)+1\right), \tag{3}$$

and causes it to buckle. Note that λ_i varies linearly through thickness. The wrinkle deformation of each layer is characterised by the function $w_i(x_i)$, which measures the displacement of the i-th layer away from radius R_i in the normal direction.

Motivated by the micrograph of Fig. 1 (right), it is assumed that the wrinkle deformation of the layer decays to zero at the tool face, with the amplitude varying as the square root of the distance from the tool surface. Consequently the complete deformation of the laminate can be written in terms of the displacement of the outermost layer, characterised by a single function $w = w_1$, where

$$w_i = \sqrt{\frac{2(N-i)+1}{2N-1}}w. \tag{4}$$

This mode is chosen through-thickness so that, for a given wrinkle deformation w, each layer remains compatible with the bookend/loading constraint (see Section 2.2.3). The setup of the model can be simplified to a single layer of effective elastic stiffness $\hat{B}$ laid around the corner radius $R(\eta) = R_1$, as seen in Fig. 2 (i). Wrinkle deformations w away from R are resisted by a nonlinear Winkler foundation which acts strictly locally and normal to the layer. This encapsulates the work done in wrinkling, as the material squashes internally, and is connected to the consolidation law (1). A single rigid load p mimics the combined effect of all loads p_i, preventing them from slipping.

A total potential energy is now calculated from which a critical wrinkling/buckling load $p = p^c$ and associated buckling wavelength is derived.

2.2.1 Bending Energy, U_B

Each layer is assumed identical with bending stiffness B, therefore the strain energy due to bending is

$$U_{B_i} = \frac{1}{2}B\int_{-\frac{1}{2}\ell_i}^{\frac{1}{2}\ell_i}\kappa_i^2\,dx_i. \tag{5}$$

where κ_i defines the curvature of the i^{th} layer. Since the wavelengths of the wrinkle deformations are small, changes in curvature of the mid-surface of i^{th} layer can be approximated by

$$\kappa_i \simeq \frac{d^2w_i}{dx_i^2} \tag{6}$$

see for example Thompson and Hunt [20]. The strain energy stored in bending of the laminate is therefore the sum of the bending energy of all layers,

$$U_B = \frac{1}{2}\sum_{i=1}^{N} B \int_{-\frac{1}{2}\ell_i}^{\frac{1}{2}\ell_i} \left(\frac{d^2 w_i}{dx_i^2}\right)^2 \, dx_i. \tag{7}$$

By applying (4) and noting that

$$\mathrm{d}x_i = \frac{R_i}{R_t}\,\mathrm{d}x_t \quad \text{and} \quad \frac{dw_i}{dx_i} = \frac{dw_i}{dx_t}\frac{dx_t}{dx_i} = \frac{dw_i}{dx_t}\frac{R_t}{R_i} \tag{8}$$

it follows that

$$U_B = \frac{1}{2}\sum_{i=1}^{N} B \int_{-\frac{1}{2}\ell_t}^{\frac{1}{2}\ell_t} \left(\frac{R_t}{R_i}\right)^4 \left(\frac{d^2 w_i}{dx_t^2}\right)^2 \frac{R_i}{R_t} dx_t = \frac{1}{2}\hat{B} \int_{-\frac{1}{2}\ell_t}^{\frac{1}{2}\ell_t} \left(\frac{d^2 w}{dx_t^2}\right)^2 \, dx_t, \tag{9}$$

such that

$$\hat{B} = B\sum_{i=1}^{N} \frac{2(N-i)+1}{2N-1}\left(\frac{R_t}{R_i}\right)^3. \tag{10}$$

The subscript t refers to the tool surface, whereas w is the deflection of the outermost layer (see Figure 3).

2.2.2 Foundation energy, U_F

The pre-buckled state is uniform consolidation η of the corner radius such that the wrinkle displacement $w \equiv 0$. It follows from (1) that for a given consolidation pressure q,

$$\eta = \sqrt{q/C}.$$

The aim of the model is to find the bifurcation point at which the plies wrinkle; therefore the energy formulation captures the work done by an infinitesimal displacement w away from the pre-stressed state. The resistance of the laminate and the consolidation pressure to the initial buckling response can be captured by a linear spring with a stiffness measured from the prestressed state η (as shown in [20]). This spring captures both the work done against the consolidation pressure and the work done into the laminate, to the leading order. The laminate stiffness about the this state can found by differentiating (1) with respect to η, $\mathcal{S}(\eta) = 2C\eta$. The linear spring stiffness of the laminate in response to a wrinkling displacement w, is found by expanding $\mathcal{S}$ about the equilibrium position $\eta - w/Nh$ and taking only leading order terms, so that

$$f(w) = 2C\eta w = 2\sqrt{Cq}\, w. \tag{11}$$

The associated total elastic strain energy stored in the Winkler foundation is

$$U_F = \int_{-\frac{1}{2}\ell_1}^{\frac{1}{2}\ell_1} \frac{1}{2} 2C\eta w^2 \, dx_1 = \frac{R_1}{R_t}\int_{-\frac{1}{2}\ell_t}^{\frac{1}{2}\ell_t} C\eta w^2 \, dx_t. \tag{12}$$

Once buckled this simplification no longer holds, and the post-buckling response would become nonlinear and strongly asymmetric, doing work against consolidation pressure in one direction and into a stiffening foundation in the other. For this case both expressions would need to be included in the energy formulation, and so it remains outside the scope of the buckling analysis presented in this paper.

2.2.3 Loading constraint, Δ

As the laminate consolidates, a load p prevents the layers from shearing over one another, Fig. 2. This can be imposed on the model by applying the rigid loading constraint. Since each layer is assumed inextensible the original length of the layer over the corner radius is equal to length of the wrinkled layer once the laminate has consolidated, i.e for the outside layer

$$\frac{1}{2}\pi R_1(0) = \int_{-\frac{1}{2}\ell_1}^{\frac{1}{2}\ell_1} \sqrt{1+\left(\frac{dw}{dx_1}\right)^2}\, dx_1 = \frac{R_1}{R_t}\int_{-\frac{1}{2}\ell_t}^{\frac{1}{2}\ell_t} \sqrt{1+\left(\frac{R_t}{R_1}\frac{dw}{dx_t}\right)^2}\, dx_t. \tag{13}$$

Applying equation (3) and making the small displacement approximation

$$\sqrt{1+\left(\frac{dw}{dx}\right)^2} \simeq 1 + \frac{1}{2}\left(\frac{dw}{dx}\right)^2,$$

the constraint can be written as

$$\Delta = \frac{1}{2}\frac{R_t}{R_1}\int_{-\frac{1}{2}\ell_t}^{\frac{1}{2}\ell_t} \left(\frac{dw}{dx_t}\right)^2 \, dx_t. \tag{14}$$

The unknown load p is to be found as part of the solution.

2.3 Total potential energy and buckling analysis

The linearised total potential energy of the system is the sum of work done in bending and into the foundation , minus the work done by the load p in preventing the outer layer from slipping a distance λ_1, given by

$$V = U_B + U_F - p\Delta = \int_{-\frac{1}{2}\ell_t}^{\frac{1}{2}\ell_t} \left[\frac{1}{2}\hat{B}\left(\frac{d^2w}{dx_t^2}\right)^2 - \frac{1}{2}p\frac{R_t}{R_1}\left(\frac{dw}{dx_t}\right)^2 + \frac{R_1}{R_t}C\eta w^2 \right] dx_t. \tag{15}$$

The critical condition for a wrinkle corresponds to the linear buckling load of the system. This is found by seeking stationary solutions of the total potential energy (15) of the form $w(x) = A\cos(\pi x_t/\xi)$. Inserting this mode into (15) yields

$$V(\xi, A) = \frac{1}{2}\hat{B}\ell_t\left(\frac{\pi}{\xi}\right)^4 A^2 - \frac{1}{2}\frac{R_t}{R_1}p\ell_t\left(\frac{\pi}{\xi}\right)^2 A^2 + \frac{R_1}{R_t}C\eta\ell_t A^2. \tag{16}$$

Stationary solutions of V with respect to the amplitude A are solutions of

$$\frac{\partial V}{\partial A} = A\ell_t\left(\hat{B}\left(\frac{\pi}{\xi}\right)^4 - p\frac{R_t}{R_1}\left(\frac{\pi}{\xi}\right)^2 + 2C\eta\frac{R_1}{R_t}\right) = 0 \tag{17}$$

Therefore either $A = 0$, the trivial unbuckled state, or

$$p^c = \frac{R_1}{R_t}\frac{\hat{B}\pi^2}{\xi^2} + \frac{2C\eta\xi^2}{\pi^2} \tag{18}$$

and the laminate buckles. Finding the stationary value of this critical load with respect to the half wavelength ξ, i.e solving $\partial p^c/\partial\xi = 0$ for ξ, gives the half wavelength

$$\xi^c = \pi\sqrt[4]{\frac{\hat{B}R_1}{R_t 2C\eta}} \tag{19}$$

which corresponds to the lowest critical load p^c.

2.4 Critical limb length: derivation of a design criterion to produce wrinkling free corner radii

The analysis has considered the case in which a wrinkle has formed; however this may not be the case if the excess length can be accommodated by generating bookends as described by the mechanisms in Section 1 and Fig. 2. Furthermore it is useful to derive design criteria by which to compare the different modelling inputs and understand the influence of each of the parameters in causing wrinkles. A critical condition can be derived, such that if

$$\tau^c < \tau(\gamma), \tag{20}$$

i.e. if the shear stress τ^c associated with the buckling load p^c is less than the shear stress required to shear the limbs $\tau(\gamma)$, a wrinkle will form. Here γ denotes the shear strain required to accommodate the length. The shear stress through the laminate, $\tau = \delta p/h = (p_i - p_{i+1})/h$, is assumed to be constant (see Section 2.2.3) where δp is the difference in the loads acting on two adjacent plies. The buckling load p^c can be related to the loads acting on each layer, by taking moments about point E in Fig. 3 as follows:

$$p\,(R_1 - R_t) = \sum_{i=1}^{N} p_i\,(R_i - R_t) \quad \text{such that} \quad p_i = p_1\frac{2(N-i)+1}{2N-1}. \tag{21}$$

The shear stress and strain are

$$\tau^c = \frac{\delta p^c}{L} = \frac{p_i^c - p_{i-1}^c}{L} = \frac{p_1}{2N-1} \quad \text{and} \quad \gamma = \frac{\delta\lambda}{h} = \frac{\lambda_i - \lambda_{i-1}}{h}, \tag{22}$$

where the constant $\delta p^c = p_i^c/(2N-1)$ is calculated by combining equations in (21) for a known p^c. The inequality can be rearranged to derive a critical limb length

$$L_{crit} = \frac{\delta p^c}{\tau(\gamma)}, \tag{23}$$

such that if $L > L_{crit}$ a laminate will wrinkle. In the sections which follow two forms for $\tau(\gamma)$ are considered, a simple coulomb friction type model and linear elastic model respectively given by the following relationships

$$\tau_f(\gamma) = \mu q \quad \text{and} \quad \tau_e(\gamma) = G\gamma. \tag{24}$$

Here μ is the coefficient of friction, q is the consolidation pressure and G is the elastic shear modulus.

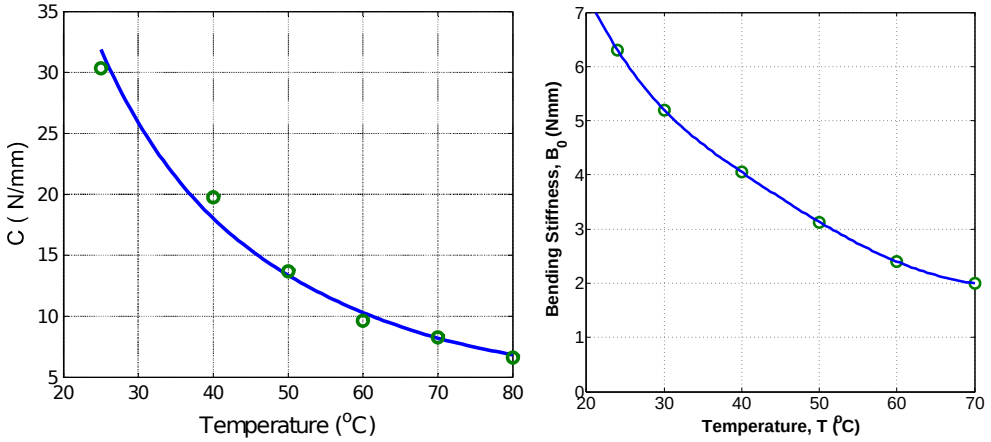

Figure 4: (Left) Plot of consolidation coefficient C against temperature T. (Right) Plot of bending stiffness of a single uncured layer of AS4/8552 in the fibre direction B_0 against temperature T.

3 Experimental data for determining modelling parameters

For comparison with wrinkle deformations in section 4 we derive modelling parameters for uncured 8552 carbon fibre prepreg. The initial thickness t of the uncured carbon fibre prepreg are measured pre-consolidation; with a mean values of $t = 0.20$mm. All other geometric parameters, e.g. R_t and N, are stated for each calculation.

3.1 Elastic consolidation, C

The elastic behaviour of the lamina under compaction was characterized by consolidating six separate specimens at four distinct strains, with the experiments being repeated at six different temperatures. At each strain level, the displacement was held constant while the load settled to equilibrium. Using these relaxed loads the complete elastic response of the lamina is extracted. For this study, six cross-ply $[0, 90]_{10}$ specimens of 50mm^2 plies were compressed by an Instron-3369 within a heated oven, which controlled the compressive strain η and temperature T. The recorded loads were fitted to (1), in the least-squared sense. Figure 4 (left) shows a plot of consolidation coefficient C against temperature T.

3.2 Elastic bending stiffness of uncured carbon fibre laminates, B

The bending stiffness in the fibre direction of single uncured ply of AS4/8552, denoted B_0 can be approximated using Dynamic Thermo Mechanical Analysis (DMTA). Here, a short length (10mm) of 8552 is clamped at both ends and subjected to a small vertical oscillation of 0.01mm at 1Hz. The DMTA machine records the load, which can be converted into an elastic bending stiffness under the assumption that plane section remain plane and shear deformation is minimal. The temperature of the experiment can be ramped from $23 - 100^o$C providing approximate values for the bending stiffness in the fibre direction B_0 as a function of temperature, as shown in Fig 4 (right).

Such experiments are prone to various sources of error; for example, gripping conditions, influence of sample length and errors in measuring small loads due to the compliance of the samples in bending. Various checks were carried out to minimise these errors. Firstly, four repeats were carried out to check consistency of results. Secondly, due to through-thickness shear, the bending stiffness becomes dependent on sample length. Therefore sample lengths are taken to be similar to the wavelengths of the expected wrinkles, to minimise the influence of this effect.

The experiment gives B_0, which can be converted to the average bending stiffness to reflect the stacking sequence of the laminate. It follows from classical laminate theory that under plane strain assumptions the bending stiffness of ply oriented θ to the original fibre direction is approximated by $B_\theta = \cos^4\theta B_0$. Therefore if α_0, $\alpha_{\pm 45}$ and α_{90} denote the percentages of 0^o, $\pm 45^o$ and 90^o plies respectively, the bending stiffness B is taken such that

$$B = \left(\alpha_0 \cos^4(0) + \alpha_{\pm 45} \cos^4(45^o) + \alpha_{90} \cos^4(90^o)\right) B_0 = \left(\alpha_0 + \frac{1}{4}\alpha_{\pm 45}\right) B_0. \tag{25}$$

3.3 Laminate shear properties, $\tau(\gamma)$

The shearing of the interface between two plies, termed *interply shear*, has been investigated experimentally [7, 14]. In each paper a central plate wrapped in unidirectional carbon fibre prepreg is clamped with a pressure by two

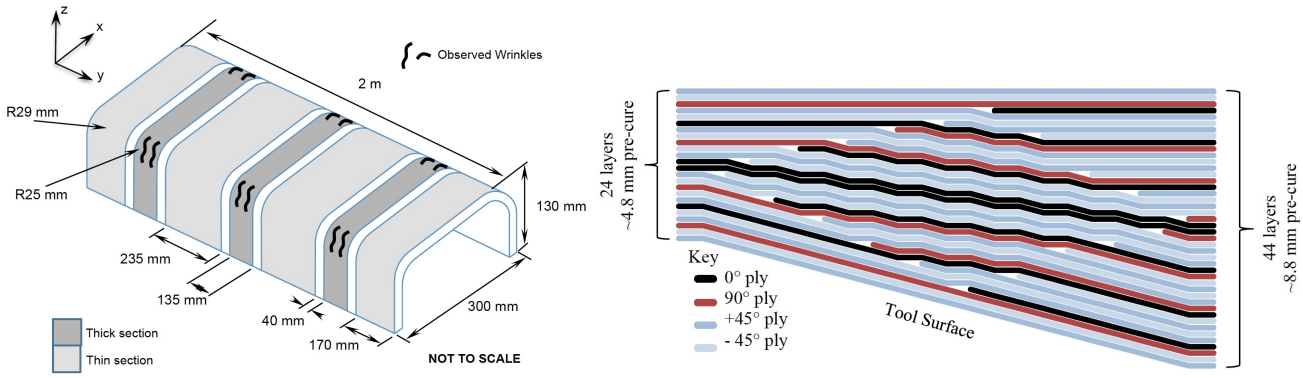

Figure 5: (Left)A schematic drawing of the 3-ramp demonstrator spar for comparision of corner radius wrinkles with model presented. (Right) Shows the symmetric stacking sequence used throughout the 3-ramp demonstrator spar: including the thin, thick and ramped regions.

side plates also wrapped in prepreg. A pneumatic cylinder generates the clamping pressure, whilst an Instron testing machines pulls the upper frame vertically at a constant rate 0.1mm/min [14], causing the layers to shear over one another. A load cell records the load required to achieve this. The setup is placed inside a heating stage to maintain a constant temperature T. The output of these experiments are compared with a simple coulomb type model, in which each ply is assumed to deform as a rigid block and the shear is achieved solely by yield of the interface, giving a coefficient of friction $\mu = 0.05 - 0.15$ [14] for 8552 resin over a range of temperatures $45 - 70^o$C. A linear elastic model is also considered (24) for shear moduli of $G = 45 - 70$kPa [5, 16], the shear modulus for uncured epoxy resin. As with the frictional coefficients, the range of values reflects the range of temperatures, as well as some uncertainty in the values due to limited experimental data. These points are discussed further in the results, where the influence of varying such parameters is considered.

4 Results

In this section the modelling results for both wrinkle wavelengths and critical limb lengths for a demonstrator spar are presented. The influence of modelling parameters on both wrinkle wavelength and critical limb length is discussed. In light of these results possible manufacturing strategies to reduce the likelihood of wrinkles are presented.

4.1 Comparisons of wrinkle wavelengths predicted by the model and observed in a large scale demonstrators

A comparison is made between predicted wavelengths and observed wrinkles in a 2m long spar demonstrator. The spar demonstrator was made up of three identical ramp sections, with dimensions as indicator in Fig. 5 (left), laid up using a Coriolis AFP robot. The thick and thin sections were made up of 44 and 24 layers of AS4/8552 respectively, connected by 1 : 10 ramps. Figure 5 (right) shows the stacking sequences used in the thick, thin and ramped regions. The corner radius of the thick section was $R_t = 25$mm, compared with $R_t = 29$mm in the thin sections. A constant limb length of $L = 100$mm was maintained along the length of the demonstrator. After all plies were laid, a single debulk at 55^oC for 15mins was performed, followed by a typical 2 hour cure cycle up to 180^oC.

Wrinkles were observed in each corner radius of the thick sections of the demonstrator, none in the thin sections. Figure 1 (right) shows a CT image in the $x - z$ plane of one such wrinkle. The half wavelength of the outermost ply was measured with an average of $\xi^c_{outer} = 5.55$ mm and standard deviation of 0.53, the measurements of each wrinkle are provided in Table 1. The observed wrinkles in the thick section were compared with the model, by noting that $\xi^c_{outer} = (R_1/R_t)\xi^c$. Modelling parameters used for comparison against the experiments can are summarised in Table 2. Applying equation (19) the model predicts a buckling half wavelength of $\xi^c_{outer} = 6.23$mm in the thick section.

In seeking to produce wrinkle free parts, critical wrinkling conditions may be of greater importance for design. However a comparison of predicted wrinkle wavelengths against those observed in the demonstrator gives confidence in the model presented, and the choice of modelling parameters (Section 3). The model shows good agreement with wrinkles in the spar demonstrator, predicting a wavelength with an average over-estimate of 10.90%. The over-estimate of the buckling wavelength is expected since, the assumed mode through thickness of the wrinkle (described by (4)) restricts the allowable degrees of freedom of the system. Consequently this

Wrinkle #	1	2	3*	4	5	6	Average (mm)	Std. Deriv (mm)
ξ^c_{outer} (mm)	4.88	6.29	5.47	5.34	5.10	6.22	5.55	0.53

Table 1: Half-wavelengths of six measured wrinkles observed in the demonstrator. Each demonstrated the same mode of wrinkling, as observed in Fig. 1 (right) which corresponds to wrinkle marked $*$.

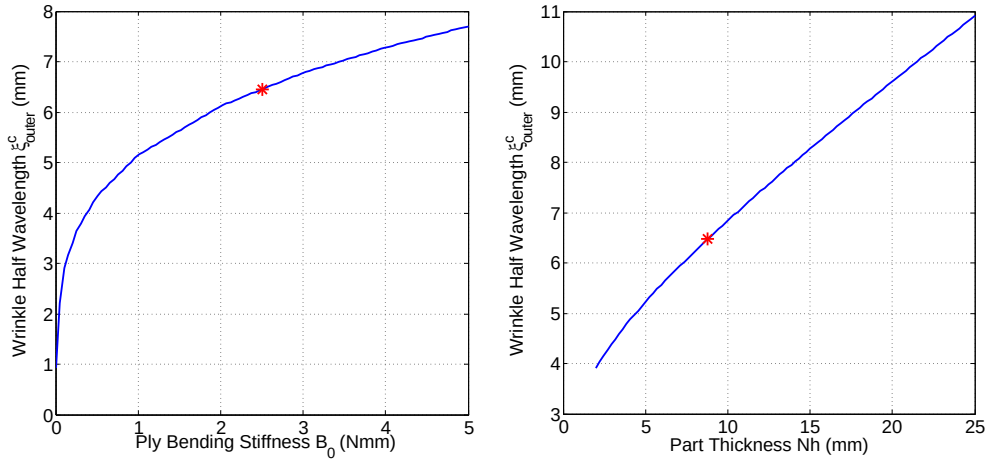

Figure 6: Influence of ply bending stiffness B_0 (left) and Part Thickness Nh (right) on critical buckling wavelength ξ^c_{outer}. With the expection of the parameters being varied, values are as in Table 2. In each plot a red '*' indicates the predicted buckling half wavelength ($\xi^c_{outer} = 6.23$mm) for the thick section of the spar demonstrator.

modelling approximation *stiffens* the system, leading to longer wavelengths than observed. The verification of the model is against a single spar demonstrator in which six wrinkles were observed and compared with the model presented. Therefore definitive conclusions cannot be made until further experimental comparisons are available for different materials and geometries. Nevertheless, this initial experimental investigation provides promise that the simple model captures the main features governing out-of-plane wrinkling during consolidation over an external corner radius. By studying the influence of each of the parameters on wrinkle wavelength and critical limb length, it is possible to see how various parameters affect the likelihood of wrinkle defects forming.

4.2 Parameteric influence on wrinkle wavelength ξ^c

Figure 6 shows how ξ^c varies for increasing bending stiffness B and part thickness Nh. Note that ξ^c is strictly increasing with respect to B. For greater B the strain energy due to bending tends to dominate, and the system counteracts this by seeking solutions of greater wavelength. The influence of part thickness on ξ^c_{outer}, Fig. 6 (right), is more complex due to the interdependencies on the parameters $\hat{B}$ and R_1, which affect ξ^c in conflicting ways. Since ξ^c is increasing with part thickness it follows that the laminate bending stiffness $\hat{B}$ is the dominant term over R_1, within this range of parameters. Intuitively, as for bending stiffness of a single ply B, a greater laminate stiffness $\hat{B}$ will give longer wavelengths.

4.3 Parametric influence on critical limb length L_{crit} and manufacturing strategies to minimise wrinkling

Following the analysis presented in section 2.4 critical limbs lengths are calculated for the coulomb friction and elastic interply shear models, in both the thick and thin sections. The results are summarised in table 3. Critical limb lengths are calculated for a range of possible values ($\mu = 0.05 - 0.15$ and $G = 45 - 70$kPa) to reflect the uncertainty in these parameters (see section 3.3). The model predicts that a wrinkle will form if $L > L_{crit.}$. In all cases the model predicts a wrinkle in the thick section, as observed. For the thin section for $\mu = 0.05$ and $G = 45$kPa the model correctly predicts the corner will be wrinkle free. For higher values of both μ and G, the

Parameter	N	R_t (mm)	h (mm)	C (N/mm)	q (N/mm)	B (Nmm)	α_0	$\alpha_{\pm 45}$
Value	44	25.0	0.20	12.5	0.10	0.86	8/44	28/44

Table 2: Geometric and material parameters used for experimental comparision at $T = 55^o$C. Note that $B = (\alpha_0 + 0.25\alpha_{45})B_0 = (8/44 + 0.25 \times 28/44) \times 2.51\text{Nmm} = 0.86\text{Nmm}$.

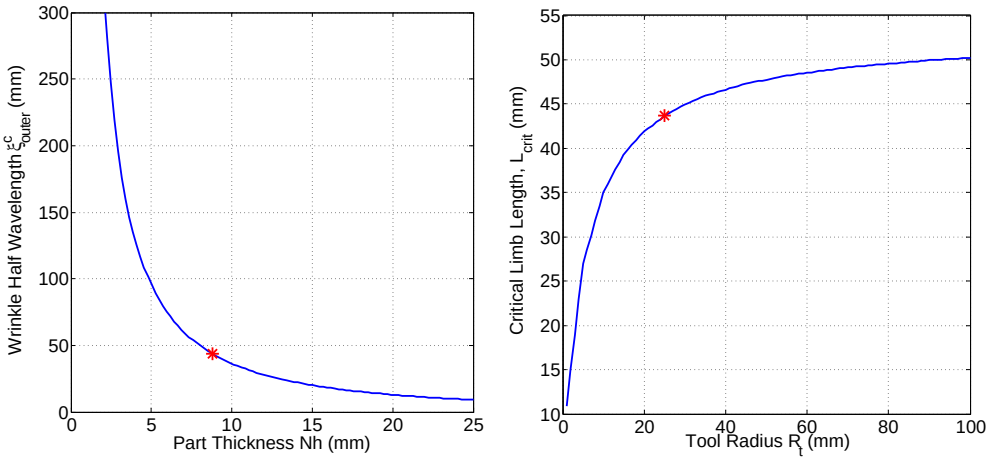

Figure 7: Influence of part thickness Nh (left) and tool radius on R_t on critical limb length L_{crit}. With the expection of the parameter being varied, values are as in Table 2 and $G = 45$kPa. In each plot a red '*' indicates the predicted critical limb lengths for the thick section ($L_{crit} = 43.67$mm) of the spar demonstrator.

model conservatively predicts wrinkles will form in the thin section. To draw further conclusions not only do further experimental comparisons need to made, but a more detailed study of the shearing of uncured carbon fibres is required, both with more complex rheological models and taking into account the effects of temperature and cure history. However the concept of critical limb length shows potential in providing criteria by which the possibility out-of-plane wrinkle defects could be minimised at the design stage.

	$\mu = 0.05$	$\mu = 0.10$	$\mu = 0.15$	$G = 45$kPa	$G = 57.5$kPa	$G = 70$kPa
Thin	132.63*	66.31	44.21	115.19*	90.15	74.05
Thick	50.29	25.15	16.76	43.67	34.18	28.07

Table 3: Critical limb length L_{crit}(mm) for a range of possible shear parameters. Note that limb length $L = 100$mm for the spar demonstrator, here * denotes wrinkle-free cases.

Independent of the choice of shear model, the new generation of 'no-flow' carbon fibre pre-pregs (e.g. M21 and 3911/2) have flow restrictors which significantly increase inter and intra-ply shear stiffness, thereby limiting the propensity to produce book-ends i.e. decreasing critical limb length L_{crit}. New material design should take into account their suitability for manufacture. Furthermore work by Larberg. *et al.* [14] shows resistance to inter or intra ply shear is minimal at $60 - 80^oC$. Whilst further investigation into the shear mechanisms of uncured materials is required, consolidation processes should be carried out at these *optimal temperatures* to provide least shear resistance.

The analysis allows us to observe how critical limb length varies with various modelling parameters, thereby identifying possible manufacturing strategies to minimise the occurrence of wrinkles. Figure 7 shows how critical limb length varies with part thickness Nh and tool radius R_t. The results show that part thickness Nh strongly affects critical limb length L_{crit}. For a thicker part greater length must be accommodated during consolidation, leading to a greater risk of generating wrinkle defects. The effect of increasing part thickness appears to have a much stronger effect than decreasing tool radius R_t. This can be seen by comparing range values of L_{crit} for varying either Nh or R_t in Fig. 7. During the manufacturing process, the part thickness can be effectively reduced by performing the consolidation in stages. After an intermediate debulk, additional plies are laid onto a well consolidated laminate, and the subsequent debulk has the benefits of decreasing part thickness whilst increasing the effective tool radius, each of which increase critical limb length.

4.4 Limitations of modelling and future work

The model presented can be seen as a first step in developing a series of models to capture the formation of defects during consolidation and curing processes. Important extension will be:

Influence of layup: Hallander *et. al* [10] shows that laminate stacking sequence plays a key role during the formation of out-of-plane wrinkles in diaphragm forming processes. The effects of layup has not been fully investigate in this contribution, whereby its influence is only included in an averaged bending stiffness B. The stacking sequence affects critical limb lengths, since L_{crit} strictly increases with ply bending stiffness B. This is expected since the associated buckling load p^c and therefore δp^c increases with B. This result suggests that

0^o layups (in which fibres run around the corner radius) might best prevent wrinkles, since the bending stiffness of a 0^o degree ply is greater than of a $\pm 45^o$ and 90^o. This conclusion may not follow, since the model assumes the layers are inextensible; if however the corner radius is made up of 90^o plies the additional length may be accommodated in-plane at sub-critical loads.

Multi-physics: In this contribution only the elastic buckling and consolidation has been considered, making the assumptions that the time of consolidation is sufficiently long that the elastic behaviour prevails, whilst temperature is assumed constant throughout the part. Both resin flow and temperature (and therefore cure kinetics) play a key role in consolidation and cure behaviour. The model will be extended to capture such effects, however in this contribution the primary focus has been to capture the effects geometric consolidation coupled with elastic buckling mechanisms.

3D geometric features: The directional nature of different plies throughout a laminate means that in directions orthogonal to the fibre directions plies may offer little or no bending stiffness, yet may be heavily constrained by consolidation in the perpendicular direction. These interactions will require the careful development of new analytical tools. We believe these are key factors in fully understanding the formation of wrinkling in carbon fibre composites during manufacture of large components.

5 Concluding Remarks

Models for process simulation are urgently needed for the composites manufacturing industry. In particular, swift, yet reliable, models for wrinkling defects during prepreg consolidation are lacking - along with methods to extract the input parameters for such models. This paper presents a one-dimensional model which encapsulates the elastic buckling/wrinkling response of plies as they consolidated over a radius whilst being constrained axially. Predicted wrinkling wavelengths show good agreement with wrinkling profiles observed in a 2m long spar demonstrator. The paper introduces the notion of *book-ending*, a mechanism by which the laminate accommodates additional length during consolidation over complex geometries without the need to form wrinkles. This leads to a new concept of critical limb length: the length of limb for which the resistance to form book-ends is equal to that to wrinkle the laminate. The analysis allows us to identify the key parameters which affect the formation of wrinkling during consolidation over a corner radius. In particular it is shown that critical limb lengths L_{crit} are most strongly influenced by part thickness and laminate shear properties.

From a modelling perspective the work highlights the importance of including the individual contribution of a layer in bending. If classical laminate continuum models are adopted, the stiffness of the laminate level response swamps the localised behaviour of individual plies and incorrect results are achieved. Once plies have the freedom to bend and slip independently, they become susceptible to buckling instabilities. The model contains a number of key simplifications so the problem remains amenable to analysis, however it still captures the important mechanics of the problem presented. This model can be used as a design tool for a corner radius, a generic feature in many composite structures.

References

[1] Adams DO, Hyer MW. Effect of layer waviness on the compression fatigue performance of thermoplastic composite laminates Fatigue 1994; 16: 385-391.

[2] Beakou A, Cano C, Le Cama JB and Verney V. Modelling slit tape buckling during automated prepreg manufacturing: A local approach Composite Structures 2011; 93:2628-2635.

[3] Boisse P, Hamila N, Vidal-Salle E, Dumont F. Simulation of wrinkling during textile composite reinforcement forming. Influence of tensile, in-plane shear and bending stiffnesses. Composite Science and Technology 2011; 71: 683-692.

[4] Boon JA, Budd CJ, Hunt GW. Level set methods for the displacement of layered materials Proc. R. Soc. Lond. A 2007; 2082:1447-1466.

[5] Costa, M. L., Botelho, E. C., Paiva, J. M. F. D., and Rezende, M. C. Characterization of cure of carbon/epoxy prepreg used in aerospace field. Materials Research, 2005; 8:317-322.

[6] Dodwell TJ, Peletier MA, Budd CJ and Hunt GW. Self-similar voiding solutions of a single layered model of folding rocks SIAM J. Appl. Math 2012; 72:444-463.

[7] Ersoy N, Potter K,Wisnom MR, Clegg M. An experimental method to study the frictional processes during composites manufacturing Composites Part A 2005; 36:1536-1544.

[8] Gereke T, Dabrich O, Habner M, Cherif C. Experimental and computational composite textile reinforcement forming: a review. Composites: Part A 2013;46:1-10.

[9] Gutowski T, Morigaki T, Cai Z. The consolidation of laminate composites Journal of Composite Materials 1989; 21:12-188.

[10] Hallander P, Akermo M, Mattei C, Petersson M, Nyman T. An experimental study of mechanisms behind wrinkle development during forming of composite laminates Composites Part A 2013; 50:54-64.

[11] Hubert P, Poursartip A. A review of flow and compaction modelling relevant to thermoset matric laminate processing J. Reinf. Plast. Comp. 1998; 17:286-318.

[12] Hunt GW, Dodwell TJ, Hammond J. On the nucleation of kink and shear bands Phil. Trans. R. Soc. A. 2013; 371.

[13] Jochuma C, Grandidierb JC. Microbuckling elastic modelling approach of a single carbon fibre embedded in an epoxy matrix Composites Science and Technology 2004; 64:2441-2449.

[14] Larberg Y, Akermo A. On the interply friction of different generations of unidirectional prepreg materials of carbon/epoxy prepreg systems. Composites Part A 2011; 42:1067-1074.

[15] Lightfoot JS, Wisnom MR,Potter K. A new mechanism for the formation of ply wrinkles due to shear between plies Composites Part A 2013; 49:139-147.

[16] Malekmohammadi S, Thorpe R, Poursartip A. Adaptation of solid micromechanics for modelling curing resins in process simulations 26th ASC Annyak Technical Conference 2011; Montreal, Canada.

[17] Pandey RK, Sun CT. Mechanisms of wrinkle formation during the processing of composite laminates Composites Science and Technology 1999; 59:405-417.

[18] Potter K., Khan B, Wisnom MR, Bell T, Stevens J. Variability, fibre waviness and misalignment in the determination of the properties of composite materials and structures Composites Part A 2008; 39:1343-1354.

[19] Rosen BW. Mechanics of composite strengthening In: Fiber Composite Materials, American Society of Metals Seminar, Metal Park, Ohio, 1965.

[20] Thompson JMT, Hunt GW. A general theory of elastic stability, Wiley, London, 1973.

[21] Wriggers P. Computational Contact Mechanics Springer, Berlin, 2006.

[22] Zhu B, Yu TX, Teng J, Tao XM. Theoretical modeling of large shear deformation and wrinkling of plain woven composite. J Compos Mater 2009;43:125-38.